Far-Ultraviolet H$_2$ Emission from Circumstellar Disks

Laura Ingleby[1], Nuria Calvet[1], Edwin Bergin[1], Ashwin Yerasi[1], Catherine Espaillat[1], Gregory Herczeg[2], Evelyne Roueff[3], Hervé Abgrall[3], Jesus Hernández[4], César Briceño[4], Ilaria Pascucci[5], Jon Miller[1], Jeffrey Fogel[1], Lee Hartmann[1], Michael Meyer[6], John Carpenter[7], Nathan Crockett[1], Melissa McClure[1]

ABSTRACT

We analyze the far-ultraviolet (FUV) spectra of 33 classical T Tauri stars (CTTS), including 20 new spectra obtained with the Advanced Camera for Surveys Solar Blind Channel (ACS/SBC) on the Hubble Space Telescope. Of the sources, 28 are in the ∼1 Myr old Taurus-Auriga complex or Orion Molecular Cloud, 4 in the 8-10 Myr old Orion OB1a complex and one, TW Hya, in the 10 Myr old TW Hydrae Association. We also obtained FUV ACS/SBC spectra of 10 non-accreting sources surrounded by debris disks with ages between 10 and 125 Myr. We use a feature in the FUV spectra due mostly to electron impact excitation of H$_2$ to study the evolution of the gas in the inner disk. We find that the H$_2$ feature is absent in non-accreting sources, but is detected in the spectra of CTTS and correlates with accretion luminosity. Since all young stars have active chromospheres which produce strong X-ray and UV emission capable of exciting H$_2$ in the disk, the fact that the non-accreting sources show no H$_2$ emission implies that the H$_2$ gas in the inner disk has dissipated in the non-accreting sources, although dust (and possibly gas) remains at larger radii. Using the flux at 1600 Å, we estimate that the column density of H$_2$ left in the inner regions of the debris disks in our sample is less than ∼ 3×10^{-6} g cm^{-2}, nine orders of magnitude below the surface density of the minimum mass solar nebula at 1 AU.

[1]Department of Astronomy, University of Michigan, 830 Dennison Building, 500 Church Street, Ann Arbor, MI 48109; lingleby@umich.edu, ncalvet@umich.edu, ebergin@umich.edu, ashwinry@umich.edu, ccespa@umich.edu, fogel@umich.edu, lhartm@umich.edu, jonmm@umich.edu, ncrocket@umich.edu, melisma@umich.edu

[2]Max-Planck-Institut fur extraterrestriche Physik, Postfach 1312, 85741 Garching, Germany; gregoryh@mpe.mpg.de

[3]LUTH and UMR 8102 du CNRS, Observatoire de Paris, Section de Meudon, Place J. Janssen, 92195 Meudon, France; evelyne.roueff@obspm.fr, herve.abgrall@obspm.fr

[4]Centro de Investigaciones de Astronomía (CIDA), Mérida 5101-A, Venezuela; jesush@cida.ve, briceno@cida.ve

[5]Department of Physics and Astronomy, Johns Hopkins University, Baltimore, MD 21218; pascucci@pha.jhu.edu

[6]ETH Hoenggerberg Campus, Physics Department, CH-8093 Zurich, Switzerland; mmeyer@phys.ethz.ch

[7]Department of Astronomy, California Institute of Technology, Mail Code 249-17, 1200 East California Boulevard, Pasadena, CA 91125; jmc@astro.caltech.edu

Subject headings: accretion, accretion disks—circumstellar matter—stars: pre-main sequence

1. Introduction

Gas comprises 99% of the mass of primordial disks. As time increases, it is accreted onto the star, formed into planets, and lost by photoevaporation, leaving behind a debris disk, in which most of the mass is locked into planets and other solid bodies traced by secondary dust arising from collisions. Although the general outline of this process is agreed upon, many specific questions remain unanswered, mainly because the gas is difficult to observe. As a result, only $\sim$1% of the disk mass, the dust, has been used as a probe of the disk evolution. However, although interconnected, the evolution of gas and dust may take different paths (Pascucci et al. 2009), making observations of the gas itself necessary to understand these processes. Of particular importance are observations of the gas in the inner disk, because it sets the chemical and physical conditions for planet formation. The bulk of the gas in these cold disks is in H_2, which lacks a permanent dipole component, so the pure rotational and rovibrational lines are weak. Nonetheless, extensive surveys of these lines in primordial disks have been carried out (Bary et al. 2008; Bitner et al. 2008, and references therein), and they have been detected in a handful of objects. Searches using less abundant molecules have also succeeded and provided information on the gas in the inner region of gas-rich disks (Carr & Najita 2008; Salyk et al. 2008; Pascucci et al. 2009; Najita et al. 2008). Gas has also been searched for in disks of more evolved sources which are no longer accreting, within the age range when the transition from primordial to debris is supposed to happen, $\sim$5 - 20 Myr. In particular, Pascucci et al. (2006) looked for H_2 in the disks of several non-accreting sources and found that the amount of gas still present at 5 - 20 Myr is not large enough to form the gas giant planets at that time. This observation agrees with results indicating that the amount of hot gas in disks of non-accreting sources is decreased when compared to accreting sources (Carmona et al. 2007).

UV observations are very promising for detecting the gas. The strong stellar Lyα radiation bathes the UV thin regions of the circumstellar material and, as long as the H_2 has a temperature of a few thousand degrees, the line excites electrons to upper electronic states, which produces a plethora of emission lines in the UV when they de-excite (Herczeg et al. 2006, H06, and references therein). At the same time, the stellar high energy radiation fields eject electrons from heavy metals, and the resulting free electrons produce additional electrons by ionizing H and He atoms; these secondary electrons then excite H_2 to upper levels, resulting in a characteristic spectrum of lines and continuum in the UV (Spitzer & Tomasko 1968; Bergin et al. 2004, B0). For electron excitation to work efficiently, temperatures need to be high enough for neutral H to be present. The relatively high temperature requirements mean that the H_2 detected by these means must either to be close to the star or to be excited by shocks. UV H_2 emission has been found to be extended

in objects surrounded by substantial natal material, in the regions where the stellar outflow shocks this material, or in fast accretors, where the H_2 may arise in the high density outflow itself (H06). However, without remnant envelopes such as the objects in this study, the only known exception being T Tau, the most likely place to find the required high temperatures is in the inner disk. This makes the UV H_2 emission ideal for probing the H_2 gas in the innermost regions of disks, regions which are difficult to access by other means.

We obtained ACS/SBC prism spectra of a fair number of accreting Classical T Tauri stars (CTTS), non-accreting weak T Tauri stars (WTTS), and more evolved disks (DD), covering the interesting age range, $\sim$1 - 100 Myr. Our goal was to search for UV H_2 emission and study its evolution. The poor spectral resolution of the ACS spectra made the identification of Lyα fluorescent lines impossible. However, we were able to identify a feature around $\sim$ 1600 Å, first proposed by B04 as due mostly to electron impact excitation of H_2. In this letter we present and analyze these spectra. We show that the H_2 feature is absent in all non-accreting and evolved stars while present in all accreting stars, and use UV fluxes to give very rough estimates of upper limits for the remaining surface density of H_2 in the latter.

2. Observations

We obtained observations of 20 CTTS and 10 non-accreting and evolved targets using the Advanced Camera for Surveys Solar Blind Channel (ACS/SBC) on the Hubble Space Telescope in 2007. The observations were obtained in GO programs 10810 (PI: Bergin), 10840 (PI: Calvet) and 11199 (PI: Hartmann). Each ACS observation consists of a brief image in the F165LP filter and a longer image obtained with the PR130L prism. Images appear unresolved. Offsets between the target location in the filter and prism image, including the wavelength solution, were obtained from Larsen (2006). The target spectrum was then extracted from a 41-pixel (1.3") wide extraction window. Background count rates of 0.05 - 0.1 counts s^{-1} were calculated from offset windows and subtracted from the extracted spectrum. The absolute wavelength solution was then determined by fitting the bright C IV λ1549 Å doublet. Fluxes were calibrated from the sensitivity function obtained from white dwarf standard stars by Bohlin (2007). The spectra range from 1230–1900 Å with a 2-pixel resolution of $\sim$ 300 at 1230 Å and $\sim$ 80 at 1600 Å.

Table 1 lists the ACS targets used in this analysis and the properties of these objects. The CTTS sources include 16 objects in the Taurus-Auriga molecular cloud and four sources in the 25 Ori aggregate in the Orion OB1a subassociation. Spectral types for the CTTS in Taurus are from Furlan et al. (2006), and ages from Hartmann (2003). To correct for reddening we used the law towards the star HD 29647 (Whittet et al. 2004) and estimated A_V by de-reddening the median photometry of Herbst et al. (1994) to fit the fluxes of a standard star in the region of the spectrum

(V to J bands) where the emission is mostly photospheric[1]. We obtained accretion luminosities L_{acc} for the Taurus sources using the U band excesses following Gullbring et al. (1998), and the median U from photometry in Herbst et al. (1994). The ages, spectral types, luminosities, A_V's, and L_{acc} for the sources in 25 Ori were taken from Briceño et al. (2007); Hernández et al. (2007) and Calvet et al. (2005).

The non-accreting sources (WTTS/DD) were selected to have no evidence of accretion and to have excesses in either Spitzer Space Telescope Infrared Spectrograph (IRS) spectra or 24 and 70 μm Multiband Imaging Photometer (MIPS) photometry, indicating the presence of debris disks. The sources in the TW Hydrae Association have been identified as WTTS by spectral observations which showed Hα in emission (Webb et al. 1999) and strong Li 6707 in absorption (Kastner et al. 1997). The WTTS/DD and their properties were discussed in Carpenter et al. (2009, 2008), Hillenbrand et al. (2008), Verrier & Evans (2008), Chen et al. (2005) and Low et al. (2005). Examples of the ACS target spectra are shown in Figure 1.

We supplemented the ACS data with previously published medium and high resolution STIS data of CTTS (Calvet et al. 2004; Herczeg et al. 2002, 2004, B04). The source properties, listed in Table 1, were taken from Calvet et al. (2004) for the Orion Molecular Cloud sources, and derived as described for the ACS Taurus sources for the STIS Taurus sources. We adopt the spectral type and age from Webb et al. (1999) and A_V from Herczeg et al. (2004) for TW Hya. Accretion luminosities for the STIS sample were taken from Calvet et al. (2004) and Ingleby et al. (2009).

3. Results

Following B04, we identified a feature in the STIS spectra at 1600 Å which is due mostly to electron impact H$_2$ emission. Due to the low resolution of the ACS spectra, we used the high resolution spectrum of TW Hya (Herczeg et al. 2004) to identify this feature in the ACS spectra; in Figure 2 we compare the feature in the observed STIS spectrum of TW Hya and in the STIS spectrum smoothed to the resolution of the ACS spectra. While the H$_2$ lines are no longer observable in the smoothed spectrum, the feature at 1600 Å is.

In addition to electron impact H$_2$ emission, the flux at 1600 Å has contributions from accretion shock emission and Lyα fluorescent lines (Ingleby et al. 2009). Attempting to isolate an indicator that is due to electron impact H$_2$ emission, we measured the flux between 1575 and 1625 Å and subtracted from it the continuum and the contribution from nearby strong lines (He II 1640 Å and C IV 1550 Å). Since it is unclear how strong the emission from additional sources is at 1600 Å, we calculated the continuum in three ways. First, by joining the troughs in the spectrum on either side of the 1600 Å feature; second, by fitting a 5th order polynomial to the entire FUV spectrum; third,

---

[1]Targets with high mass accretion rate, as DL Tau and DR Tau show significant veiling at J (Edwards et al. 2006), so the estimated extinction may be in error, although it is consistent with values from Taurus.

by adopting a continuum which assumes that the rise in the spectrum at 1600 Å is due entirely to electron impact H_2 emission. Figure 2 shows the location of the subtracted continuum for each method in TW Hya, and Figure 3 shows examples of the measurements for three ACS targets. These three methods for measuring the H_2 feature luminosity were used to estimate the errors. Comparing the TW Hya spectra at both resolutions indicates that the feature luminosity decreases by ~ 2 in the low resolution spectrum because some of the flux is blended into the continuum. This error is small compared to the uncertainty in the continuum location.

Using these procedures, we measured the luminosity of the 1600 Å feature in both the ACS spectra and the STIS spectra smoothed to the resolution of ACS; the feature luminosities are given in Table 1. For the WTTS/DD, we find that the H_2 feature is not observable and the values presented in Table 1 are upper limits based on the rms fluctuations from 1575 to 1625 Å. We thus find that the H_2 feature shows only in the accreting sources. This is not an age effect; our sample includes CTTS and WTTS of similar age at ~ 10 Myr (left panel of Figure 4) but only the accreting sources show the H_2 feature. Moreover, we find a clear correlation of the strength of the feature with L_{acc} in the CTTS (right panel of Figure 4), with a Pearson correlation coefficient of 0.68, indicating that the H_2 emission depends on the accretion properties of the source and not on the age. A similar result was found in Carmona et al. (2007), where the probability of detecting near-IR H_2 lines was greater in sources with higher accretion rates.

4. Discussion

Free electrons are required for the process of electron excitation to be effective (§1). Since, in turn, high energy radiation fields are necessary to produce fast electrons, the absence of H_2 emission in the WTTS/DD could in principle be due to a low level of X-ray or EUV emission in these objects relative to the CTTS. However, Telleschi et al. (2007) found that there is little difference between the X-ray luminosities of CTTS and WTTS in their X-ray survey of pre-main sequence objects in Taurus. Even though there is a soft X-ray excess created in the accretion shock region of CTTS (Günther et al. 2007, and references therein), it does not significantly increase the X-ray production in most young stars (Telleschi et al. 2007). Similarly, Kastner et al. (1997) showed that CTTS and WTTS in the 10 Myr TW Hya Association have similar X-ray luminosities. Moreover, the X-ray luminosity does not decrease significantly over the first 100 Myr of low mass stars (Briceno et al. 1997; Kastner et al. 1997), so the CTTS and WTTS/DD in our sample should have comparable X-ray luminosities.

The EUV radiation field, including emission from approximately 100 to 1000 Å, is also responsible for the ionization of heavy atoms, contributing to the population of free electrons available to excite an H_2 molecule. The EUV is difficult to investigate because the radiation is extremely extincted by interstellar hydrogen. Alexander et al. (2005) find that the EUV flux level does not change in the first ~ 10 Myr, from studies of the ratio He II 1640/CIV 1550 Å. If we assume that the FUV level is an indicator of the strength of the EUV emission, we come to similar conclusions.

Figure 3 shows one CTTS and one DD that have the same FUV luminosity, so one would expect a strong enough EUV radiation field in both sources to create the free electrons needed to excite H_2 if it were present. However, the excess emission at 1600 Å is clearly seen in the CTTS (FP Tau) and absent in the DD (MML 36).

Since the high energy radiation fields in both CTTS and WTTS/DD are comparable in strength, the most likely explanation for the lack of H_2 emission in WTTS/DD is that there is essentially no gas in their inner disks. Given the close relationship between the H_2 feature strength and L_{acc} shown in Figure 4, our results suggest that H_2 gas dissipates in timescales consistent with the cessation of accretion; when the gas is dissipated in the inner disk, there is no material left to accrete.

We use the observations to make a rough estimate of the column density of H_2 being collisionally excited. We assume that the H_2 is emitted in an optically thin region of the disk with area A and thickness z. The emitted luminosity per unit volume is $\mathcal{E}_\lambda = h\nu\sigma_\lambda v\chi_e n_{H_2}^2$, where $h\nu$ is the energy of the emitted photon, σ_λ the H_2 cross section, v the impacting electron velocity, n_e the electron number density, χ_e the electron fraction, and n_{H_2} the number density of H_2. The expected flux at 1600 Å due to electron impact excitation is then

$$F_{1600} = \frac{h\nu\sigma_{1600}v\chi_e\Sigma^2 R^2}{16m_H z d^2}. \tag{1}$$

where Σ is the surface density of H_2 excited by electron impacts, m_H the mass of hydrogen, R the radius of the emitting region, and d is the distance. In Ingleby et al. (2009) we find that the electron excitation model that provides the best fit to the 1600 Å feature of our sample of CTTS with STIS spectra is characterized by a temperature $T \sim 5000$ K and an electron energy of $\sim$12 eV. For these values, $\sigma_{1600} = 10^{-20} \mathrm{cm^2 \mathring{A}^{-1}}$ (Abgrall et al. 1997). According to the thermal models of (Meijerink et al. 2008, M08), gas reaches $T \sim 5000$K within 1 AU of the star, which is consistent with the upper limit to the extension of the H_2 emitting region set by the STIS resolution in the case of TW Hya (Herczeg et al. 2002). We further assume that most electrons are capable of exciting H_2 and adopt $\chi_e = 5 \times 10^{-3}$, as well as $R \sim$1 AU and $z \sim$0.1 AU (M08). Using these numbers, and assuming that all the flux at 1600 Å is due to electron impact excitation, we get the estimates of Σ in Table 1, which for CTTS are consistent with predicted formation in the uppermost levels of the disk (M08).

A similar estimate can be made for the column density of electron excited H_2 in the WTTS/DD in our sample, which have some dust remaining at larger radii but no detected IR H_2 lines (Carpenter et al. 2009, 2008; Hillenbrand et al. 2008; Verrier & Evans 2008; Chen et al. 2005; Low et al. 2005). These estimates are given in Table 1. We used the flux of MML 36, which is the WTTS/DD with the highest flux at 1600 Å in our sample, to estimate the mass of H_2 inside $\sim$1 AU; we found that there must be less than 10^{-7} earth masses, 10^{-7}% of the MMSN, lower than the 0.01% of the MMSN estimated by Pascucci et al. (2006). This has important implications for the formation of terrestrial planets, especially if gas is needed to circularize orbits (Agnor & Ward 2002). Kominami & Ida (2002) theorize that at least 0.01% of the MMSN must be present during the for-

mation of proto-planets, which form around 10 Myr according to simulations by Kenyon & Bromley (2006). Our column density estimates indicate that the amount of H_2 gas present in WTTS/DD with ages of 10-100 Myr is too small to circularize the orbits of the terrestrial planets being formed at that time. Our results support the conclusion by Pascucci et al. (2006) that there must be an additional source responsible for damping eccentricities, one possibility being dynamical friction with remaining planetesimals. Another possibility is that other species of gas exist after the H_2 has been depleted, for example, C and O have been detected around the 10 Myr debris disk β Pic (Fernández et al. 2006; Roberge et al. 2006). C and O do not feel strong radiation pressure due to the low FUV flux in WTTS and therefore may remain after the H_2 has been depleted (Roberge et al. 2006).

5. Acknowledgments

REFERENCES

Abgrall, H., Roueff, E., Liu, X., & Shemansky, D. E. 1997, ApJ, 481, 557

Agnor, C. B., & Ward, W. R. 2002, ApJ, 567, 579

Alexander, R. D., Clarke, C. J., & Pringle, J. E. 2005, MNRAS, 358, 283

Bary, J. S., Weintraub, D. A., Shukla, S. J., Leisenring, J. M., & Kastner, J. H. 2008, ApJ, 678, 1088

Bergin, E., et al. 2004, ApJ, 614, L133

Bitner, M. A., et al. 2008, ApJ, 688, 1326

Bohlin, R.C. 2007, *Instrument Science Report ACS 2007-06*

Briceno, C., Hartmann, L. W., Stauffer, J. R., Gagne, M., Stern, R. A., & Caillault, J.-P. 1997, AJ, 113, 740

Briceño, C., Hartmann, L., Hernández, J., Calvet, N., Vivas, A. K., Furesz, G., & Szentgyorgyi, A. 2007, ApJ, 661, 1119

Calvet, N., Muzerolle, J., Briceño, C., Hernández, J., Hartmann, L., Saucedo, J. L., & Gordon, K. D. 2004, AJ, 128, 1294

Calvet, N., Briceño, C., Hernández, J., Hoyer, S., Hartmann, L., Sicilia-Aguilar, A., Megeath, S. T., & D'Alessio, P. 2005, AJ, 129, 935

Carmona, A., van den Ancker, M. E., Henning, T., Goto, M., Fedele, D., & Stecklum, B. 2007, A&A, 476, 853

Carpenter, J. M., et al. 2008, ApJS, 179, 423

Carpenter, J. M., et al. 2009, ApJS, 181, 197

Carr, J. S., & Najita, J. R. 2008, Science, 319, 1504

Chen, C. H., et al. 2005, ApJ, 634, 1372

Edwards, S., Fischer, W., Hillenbrand, L., & Kwan, J. 2006, ApJ, 646, 319

Espaillat, C., et al. 2008, ApJ, 689, L145

Fernández, R., Brandeker, A., & Wu, Y. 2006, ApJ, 643, 509

Furlan, E., et al. 2006, ApJS, 165, 568

Gullbring, E., Hartmann, L., Briceno, C., & Calvet, N. 1998, ApJ, 492, 323

Günther, H. M., Schmitt, J. H. M. M., Robrade, J., & Liefke, C. 2007, A&A, 466, 1111

Hartmann, L. 2003, ApJ, 585, 398

Herbst, W., Herbst, D. K., Grossman, E. J., & Weinstein, D. 1994, AJ, 108, 1906

Herczeg, G. J., Linsky, J. L., Valenti, J. A., Johns-Krull, C. M., & Wood, B. E. 2002, ApJ, 572, 310

Herczeg, G. J., Wood, B. E., Linsky, J. L., Valenti, J. A., & Johns-Krull, C. M. 2004, ApJ, 607, 369

Herczeg, G. J., Linsky, J. L., Walter, F. M., Gahm, G. F., & Johns-Krull, C. M. 2006, ApJS, 165, 256

Hernández, J., et al. 2007, ApJ, 671, 1784

Hillenbrand, L. A., et al. 2008, ApJ, 677, 630

Ingleby, L. et al., 2009, in prep.

Kastner, J. H., Zuckerman, B., Weintraub, D. A., & Forveille, T. 1997, Science, 277, 67

Kenyon, S. J., & Bromley, B. C. 2006, AJ, 131, 1837

Kominami, J., & Ida, S. 2002, Icarus, 157, 43

Larsen, S.S. 2006, *Instrument Science Report ACS-2006-02*

Low, F. J., Smith, P. S., Werner, M., Chen, C., Krause, V., Jura, M., & Hines, D. C. 2005, ApJ, 631, 1170

Najita, J. R., Crockett, N., & Carr, J. S. 2008, ApJ, 687, 1168

Meijerink, R., Glassgold, A. E., & Najita, J. R. 2008, ApJ, 676, 518

Pascucci, I., et al. 2006, ApJ, 651, 1177

Pascucci, I., Apai, D., Luhman, K., Henning, T., Bouwman, J., Meyer, M. R., Lahuis, F., & Natta, A. 2009, ApJ, 696, 143

Roberge, A., Feldman, P. D., Weinberger, A. J., Deleuil, M., & Bouret, J.-C. 2006, Nature, 441, 724

Salyk, C., Pontoppidan, K. M., Blake, G. A., Lahuis, F., van Dishoeck, E. F., & Evans, N. J., II 2008, ApJ, 676, L49

Spitzer, L. J., & Tomasko, M. G. 1968, ApJ, 152, 971

Telleschi, A., Güdel, M., Briggs, K. R., Audard, M., & Palla, F. 2007, A&A, 468, 425

Verrier, P. E., & Evans, N. W. 2008, MNRAS, 390, 1377

Webb, R. A., Zuckerman, B., Platais, I., Patience, J., White, R. J., Schwartz, M. J., & McCarthy, C. 1999, ApJ, 512, L63

White, R. J., & Ghez, A. M. 2001, ApJ, 556, 265

Whittet, D. C. B., Shenoy, S. S., Clayton, G. C., & Gordon, K. D. 2004, ApJ, 602, 29

Table 1.   Sources

Object	Spectral Type	L $L_\odot$	A_V mag	Age Myr	L_{acc} $L_\odot$	H_2 Feature $10^{-5} L_\odot$	Σ 10^{-6} g cm^{-2}
ACS CTTS							
AA Tau	M0	1.1	1.4	1	$0.13\pm^{.15}_{.03}$	$79.9\pm^{0}_{67}$	> 49.3
CI Tau	K6	1.3	2.1	1	$0.47\pm^{.34}_{.11}$	$3.3\pm^{2.0}_{0}$	> 9.9
DE Tau	M1	1.2	1.1	1	$0.16\pm^{.16}_{.05}$	$2.9\pm^{6.9}_{1.4}$	> 36.3
DL Tau	K7	1.0	1.6	1	$0.32\pm^{.26}_{.08}$	$3.3\pm^{4.1}_{2.1}$	> 22.5
DN Tau	M0	1.2	0.8	1	$0.04\pm^{.07}_{.01}$	$0.49\pm^{4.5}_{.13}$	> 18.4
DO Tau	M0	1.4	2.4	1	$0.29\pm^{.24}_{.08}$	$46.1\pm^{13}_{8.6}$	> 84.6
DP Tau	M0	0.2	0.5	1	$0.01\pm^{.02}_{.003}$	$4.2\pm^{1.9}_{1.4}$	> 17.6
DR Tau	K7	1.7	1.0	1	$1.03\pm^{.53}_{.22}$	$14.1\pm^{4.3}_{3.7}$	> 43.2
FM Tau	M0	0.5	1.9	1	$0.30\pm^{.26}_{.07}$	$16.0\pm^{6.8}_{13}$	> 61.7
FP Tau	M3	0.4	0.1	1	$0.001\pm^{.004}_{.0004}$	$0.021\pm^{.10}_{.004}$	> 4.9
GK Tau	M0	1.4	1.1	1	$0.06\pm^{.08}_{.02}$	$0.98\pm^{1.7}_{.58}$	> 18.1
HN Tau A*	K5	0.2	1.2	1	$0.07\pm^{.10}_{.02}$	$16.6\pm^{9.2}_{1.8}$	> 38.8
HN Tau B*	M4	0.03	0.9	1	–	$0.15\pm^{.53}_{.04}$	> 5.8
IP Tau	M0	0.7	0.9	1	$0.02\ \pm^{.05}_{.004}$	$0.61\pm^{2.8}_{0.4}$	> 15.0
UZ Tau A*	M1	0.3	0.5	1	$0.02\pm^{.07}_{.02}$	$0.80\pm^{2.8}_{0}$	> 14.3
UZ Tau B*	M2	0.3	1.0	1	$0.02\pm^{.07}_{.02}$	$1.5\pm^{2.9}_{.91}$	> 8.5
CVSO 206	K6	0.2	0.2	9	–	$1.2\pm^{.17}_{.51}$	> 13.9
CVSO 35	K7	0.7	0.7	9	$0.02\pm^{.01}_{.01}$	$3.2\pm^{2.3}_{2.7}$	> 16.6
CVSO 224†	M3	0.1	0.5	9	–	–	–
OB1a 1630	M2	1.0	0.0	9	–	$1.3\pm^{1.3}_{1.0}$	> 13.3
STIS CTTS							
BP Tau	K7	1.3	1.0	1	$0.23\pm^{.29}_{.20}$	$14.1\pm^{23}_{7.4}$	>41.6
DM Tau	M1	0.3	0.6	1	$0.08\pm^{.10}_{.07}$	$15.4\pm^{15}_{5.5}$	> 39.5
GM Aur	K3	1.2	1.1	1	$0.18\pm^{.21}_{.16}$	$19.7\pm^{48}_{4.9}$	> 48.7
LkCa 15	K5	1.0	1.0	1	$0.03\pm^{.06}_{.02}$	$8.6\pm^{6.8}_{2.5}$	> 26.4
RY Tau	G1	9.6	2.2	1	$1.6\pm^{2.4}_{.80}$	$338.0\pm^{400}_{120}$	> 148.4
SU Aur	G1	7.8	0.9	1	$0.10\pm^{.20}_{.01}$	$6.8\pm^{14}_{1.5}$	> 30.0
T Tau	G6	7.8	1.8	1	$0.90\pm^{1.2}_{.60}$	$104.5\pm^{37}_{18}$	> 103.9
CO Ori	G0	22.3	2.0	1	$1.7\pm^{2.5}_{.90}$	$303.5\pm^{550}_{110}$	> 149.0
EZ Ori	G3	5.9	0.6	1	$0.10\pm^{0}_{0}$	$20.0\pm^{8.5}_{7.9}$	> 41.1

Table 1—Continued

Object	Spectral Type	L $L_\odot$	A_V mag	Age Myr	L_{acc} $L_\odot$	H$_2$ Feature $10^{-5}L_\odot$	Σ 10^{-6} g cm^{-2}
GW Ori	G0	61.8	1.3	1	$4.7\pm^{6.9}_{2.5}$	$188.2\pm^{250}_{49}$	> 178.8
P2441	F9	11.5	0.4	1	$0.4\pm^{.60}_{.20}$	$3.4\pm^{3.9}_{1.8}$	> 29.0
V1044 Ori	G2	6.7	0.4	1	$0.6\pm^{.90}_{.30}$	$4.6\pm^{.30}_{3.0}$	> 37.6
TW Hya	K7	0.3	0	10	$0.03\pm^{.04}_{.02}$	$2.6\pm^{3.1}_{.92}$	> 43.9
ACS WTTS							
HD 12039	G4	–	0	31.6	0	$<.021$	< 2.2
HD 202917	G5	0.7	0	31.6	0	$<.016$	< 2.8
HD 61005	G8	0.6	0	125.9	0	$<.013$	< 1.3
HD 92945	K2	–	0	20 - 150	0	$<.006$	< 0.93
HD 98800	K5	0.6	0	10.0	0	$<.019$	< 0.84
MML 28	K2	–	0.1	15.8	0	$<.015$	< 2.4
MML 36	K5	–	0.3	15.8	0	$<.042$	< 3.3
TWA 7	M1	0.31	0	10.0	0	$<.003$	< 1.0
TWA 13A	M1	0.18	0	10.0	0	$<.016$	< 1.5
TWA 13B	M1	0.17	0	10.0	0	$<.002$	< 1.5

Note. —

[*] Stellar properties for binaries are from White & Ghez (2001). UZ Tau A and B are themselves binaries; UZ Tau A is a spectroscopic binary and UZ Tau B is a binary system (White & Ghez 2001) but is unresolved by ACS/SBC.

[†] CVSO 224 is a CTTS surrounded by a transitional disk (Espaillat et al. 2008) and has a very low $\dot{M}$. The ACS/SBC spectrum of this target is noisy and while we cannot confidently quantify the H$_2$ emission, we do see the rise in the spectrum at 1600 Å which indicates its presence.
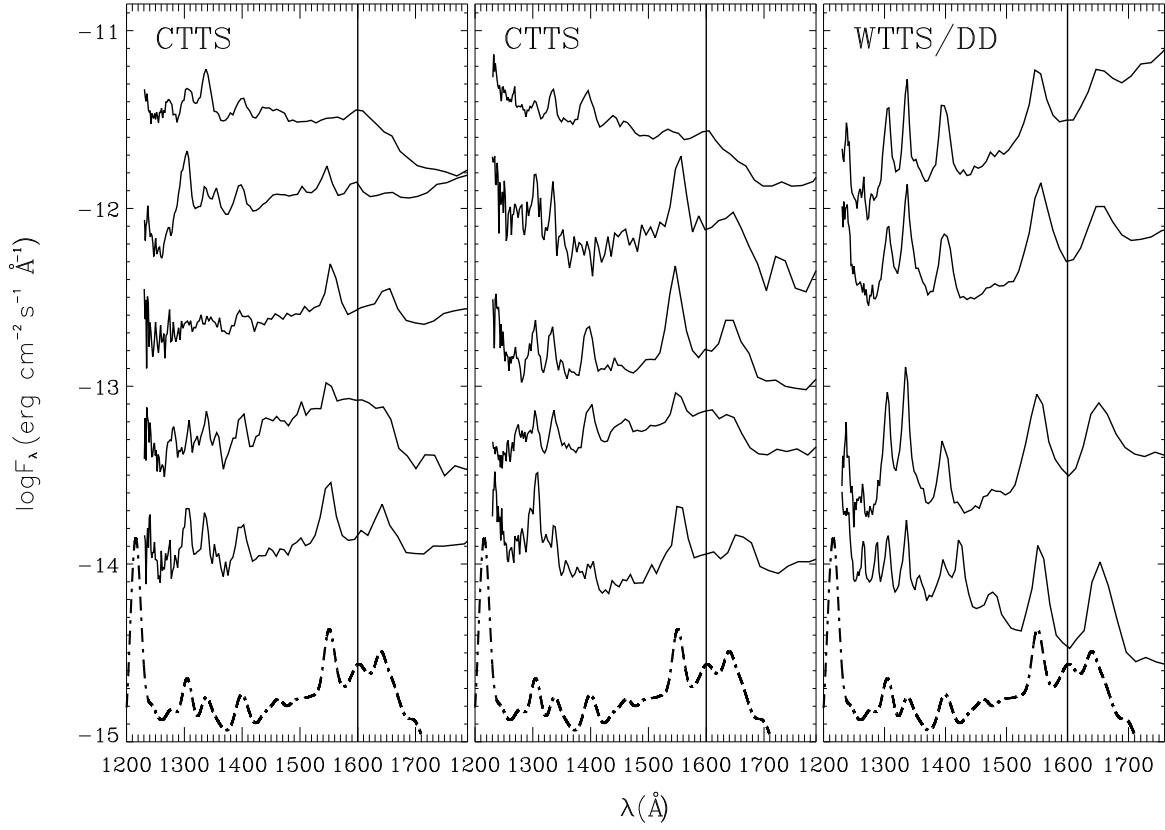
Fig. 1.— Sample of ACS CTTS spectra. Spectra have been corrected for reddening using the values of A_V listed in Table 1. Spectra have been scaled vertically for clarity. The bottom spectrum (dash-dotted line) in each panel is the STIS TW Hya spectrum smoothed to the resolution of the ACS spectra for comparison and offset by -1.2. The vertical line at 1600 Å marks the center of the feature used to identify the H_2. Left panel, from top to bottom including the offset in parenthesis: DP Tau (+2.7), DR Tau (+1.5), FM Tau (+0.5), FP Tau (+2.2) and GK Tau (+0.3). Middle panel; from top to bottom: HN Tau A (+1.9), HN Tau B (+3.0), IP Tau (+1.5), UZ Tau A (+1.2) and UZ Tau B (+0.45). The right panel shows ACS spectra of WTTS/DD; from top to bottom: HD 12039 (+3.4), HD 202917 (+2.5), HD 61005 (+2.0), HD 92945 (+1.7) and HD 98800 (+0.8).
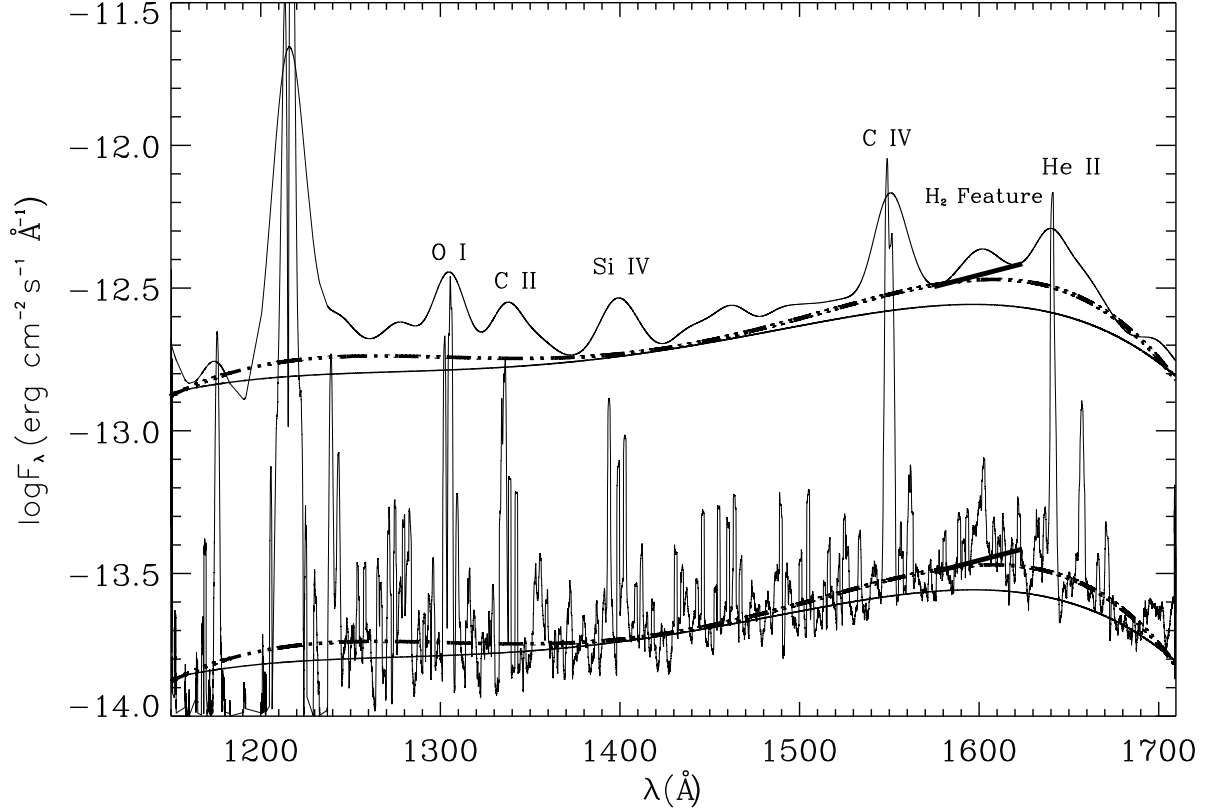
Fig. 2.— Observed and convolved spectra for TW Hya. The bottom spectrum is the high resolution STIS FUV spectrum. The top spectrum is the TW Hya spectrum convolved to the ACS spectral resolution and offset by +1.0. The solid and dashed lines on the smoothed spectrum show the three subtracted continua. These three continua are also shown plotted on the high resolution spectrum and indicate that the lowest continuum may provide the best measure of the luminosity. The strong emission lines are labeled along with the H_2 feature.
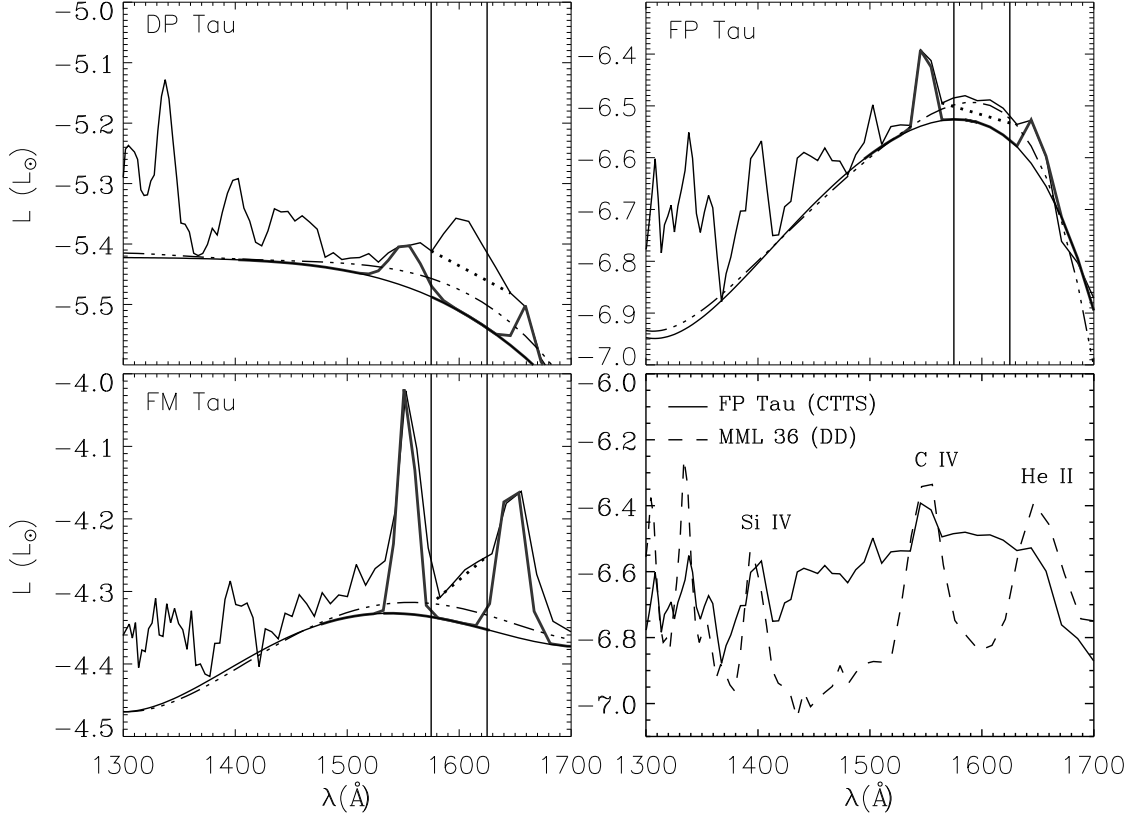
Fig. 3.— H$_2$ measurements for ACS sources. The first three panels show ACS sources and the location of the subtracted continua, shown as the solid, dashed and dot-dashed lines. Also plotted are the He II and C IV emission lines as the thick solid line. The final panel compares accreting and non-accreting sources with the same luminosity. An excess in FP Tau is observed at 1600 Å, which is due to electron impact H$_2$ emission, and also between the S IV and C IV lines, which is likely due to blended electron impact and Lyα fluorescent lines.
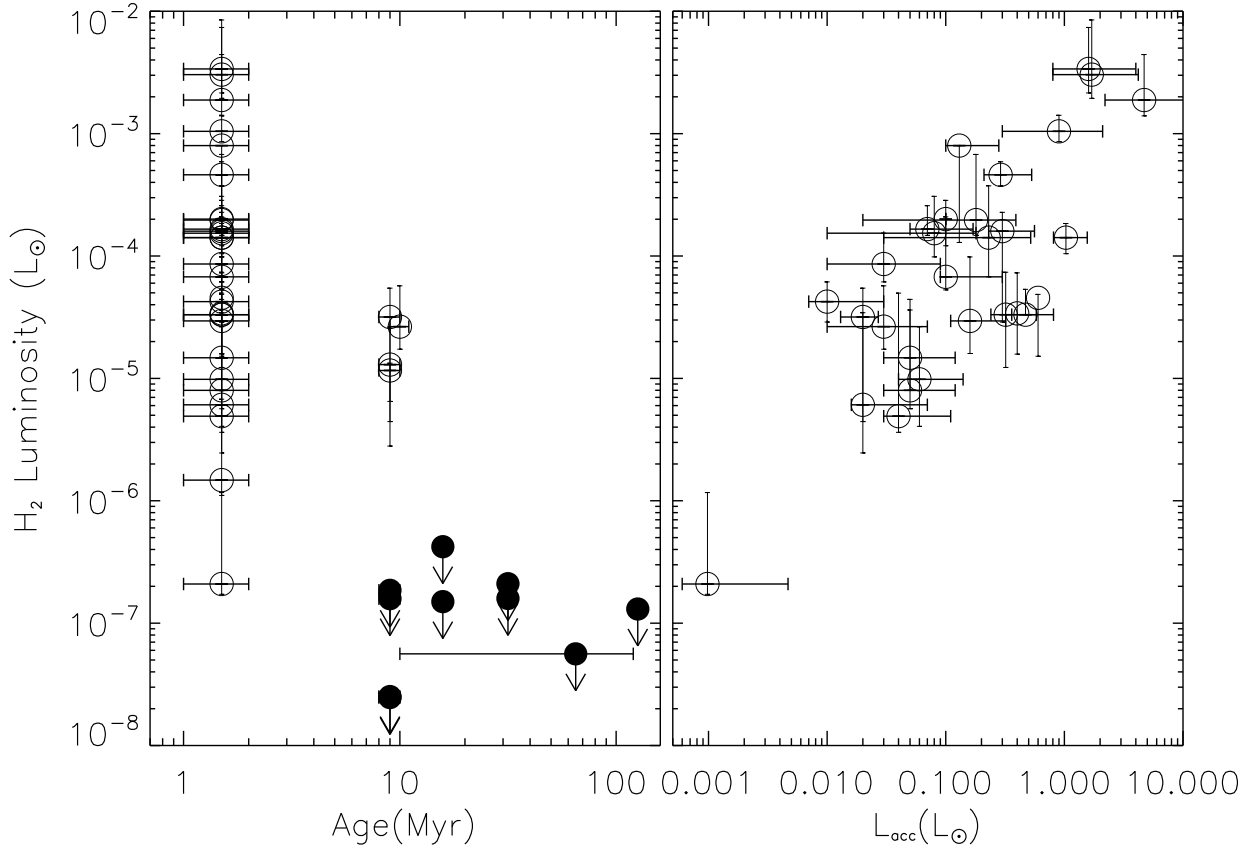
Fig. 4.— Left: Luminosity of the H_2 vs. age. Filled circles represent WTTS and open circles represent CTTS. For the WTTS we show only an upper limit on the luminosity of the H_2. Right: H_2 luminosity vs. L_{acc}. The H_2 luminosity is observed to increase with L_{acc}. Errors on L_{acc} are calculated using the scatter in the correlation with L_U presented in Gullbring et al. (1998).